Energy, Mines and Resources Canada | Énergie, Mines et Ressources Canada

CANMET

Canada Centre for Mineral and Energy Technology | Centre canadien de la technologie des minéraux et de l'énergie

MICROSTRUCTURE AND MECHANICAL PROPERTIES OF SUBMERGED ARC WELDS IN HSLA 80 STEEL FOR NAVAL APPLICATIONS

J.T. MCGRATH, J.A. GIANETTO AND R.F. ORR
WELDING SECTION

APRIL, 1987

PHYSICAL METALLURGY RESEARCH LABORATORIES

26 pp
REPORT: PMRL 87-26(TR)

PHYSICAL METALLURGY RESEARCH LABORATORIES
REPORT: PMRL 87-26(TR)

MICROSTRUCTURE AND MECHANICAL PROPERTIES OF SUBMERGED ARC WELDS IN HSLA80 STEEL FOR NAVAL APPLICATIONS

by

J.T. McGrath, J.A. Gianetto and R.F. Orr

ABSTRACT

The relationship between microstructure and mechanical properties was examined for the weld metal and heat affected zone in submerged arc HSLA80 weldments.

The weld metal, deposited over an energy input range of 2-4kJ/mm and with two wire/flux consumable combinations exceeded the targeted notch toughness properties. The superior toughness resulted from a high proportion of acicular ferrite and low inclusion content.

The notch toughness of the coarse grain heat affected zone decreased with an increase in energy input. The low toughness at the highest (4kJ/mm) energy input resulted from the formation of a coarse upper bainite microstructure.

LABORATOIRES DE RECHERCHE EN MÉTALLURGIE PHYSIQUE
RAPPORT: PMRL 87-26(TR)

MICROSTRUCTURE ET PROPRIÉTÉS MÉCANIQUES DES SOUDURES À L'ARC SUBMERGÉ DANS DES ACIERS HSLA80 POUR UTILISATIONS MARINES

par

J.T. McGrath, J.A. Gianetto et R.F. Orr

RÉSUMÉ

La relation entre la microstructure et les propriétés mécaniques a été étudiée au niveau du métal de soudure et de la zone thermiquement affectée des soudures à l'arc submergé d'un acier HSLA80.

Le métal de soudure déposé avec un apport d'énergie dans la gamme de 2-4kJ/mm et à l'aide de deux combinaisons fils/flux du commerce a dépassé les propriétés de résistance à l'entaille fixées. La résistance supérieure provenait d'une proportion élevée de ferrite aciculaire et d'une faible teneur d'inclusions.

La résistance à l'entaille de la zone thermiquement affectée à grains grossiers a diminée avec l'augmentation de l'apport d'énergie. La faible résistance relevée au cours de l'apport d'énergie le plus élevé, provient de la formation d'une microstructure bainitique grossière.

INTRODUCTION

Current interest in the fabrication of submarine pressure hulls has prompted studies on the welding of conventional high-strength quenched and tempered steels, particularly, HY80 (1) and HY100 (2). Recently attention has been directed towards alternative high-strength low alloy steels with the aim of reducing welding fabrication costs associated with the less weldable HY steels. One of these steels, designated HSLA80, is a modified version of ASTM A710 Grade A Class 3 and is currently being specified for the construction of U.S. Navy ships (3). Over the past few years, several researchers have published results on the development of A710 copper precipitation strengthened steels (4, 5).

The HSLA80 steel differs from the conventional higher carbon quenched and tempered HY steels in that the strength is obtained through copper precipitation hardening. The steel has lower carbon levels (Table 1) and therefore does not transform to the hard martensitic structure associated with the HY steels. This can provide improved weldability and toughness for the HSLA80 steel. However, the application of HSLA80 for submarine fabrication requires extensive research and development to establish its suitability as an alternative steel. Therefore, the present program was designed with the following objectives: (a) to develop submerged-arc weld (SAW) procedures to join HSLA80 steel using a series of commercially available welding consumables for a range of energy inputs, and (b) to evaluate the mechanical properties, in particular the notch toughness of both the weld metal and the coarse grain heat-affected zone (CGHAZ). The targeted mechanical properties presented in Table 2 were established from current military standards concerned with the qualification of HY80/HY100 welding consumables (6) for the submerged-arc welding process.

EXPERIMENTAL PROCEDURE

Submerged-arc welds were deposited in 25.4 mm thick HSLA80 high-strength steel using the consumables and welding parameters listed in Table 3. The range of energy inputs employed were in accordance with the current military standard for the construction of submarines using HY80/HY100 steels (7). Single-vee joint design preparations were used with a 60° included angle and a 6-8 mm land as shown in Fig. 1(a). Carbon-arc backgouging was employed on the second side prior to deposition of the final passes. All welding was done parallel to the plate rolling direction.

The tensile properties of the weld metal deposits were determined from all weld metal tensile specimens. Charpy impact energy transition curves were produced for specimens notched through-thickness at the weld centreline and in the CGHAZ (1 mm from the fusion line) on the backgouged side of each weldment (Fig. 1(b)).

The microstructures of both the weld metal and CGHAZ were characterized using optical microscopy for each welding condition. Scanning electron microscopy was employed to examine the fractured surfaces of selected Charpy specimens. Microhardness measurements were also made using a 500 g load in the vicinity of the Charpy notches at both the weld metal centreline and in the CGHAZ.

RESULTS

Weld Metal Chemistry

The chemical compositions of the submerged-arc welds are listed in Table 4, along with the corresponding wire chemistries. Variations in weld chemistry reflect the influence of dilution resulting from the varying energy input. The dilution was calculated geometrically and ranged from about 30 to 65% on the backgouged side for the 2-4 kJ/mm energy inputs. The primary differences in weld chemistry within each series were attributed to the influence of increasing energy input which resulted in a general increase in Cr and Cu and a decrease in oxygen contents.

Overall the chemistries of both series A and B welds were similar. The only difference was the higher Cu in the series B welds resulting from the copper coating of the LA100 wire.

Weld Metal and CGHAZ Microstructure

The weld metal microstructure in the root region (from which the Charpy specimens were taken) for the series A and B welds contained as-deposited and reheated regions. The proportion of as-deposited structure increased from approximately 30% for the 2 kJ/mm weldments to 100% for the 4 kJ/mm weldments. For the low energy input weld 10 passes were required to complete the joint compared with only 4 passes for the high energy (4 kJ/mm) input weld (Fig. 1(a)).

Representative micrographs of the as-deposited region of the series A and B welds are shown in Figs. 2 and 3. The microstructure within the as-deposited region was composed of a high proportion of acicular ferrite with some discontinuous grain boundary ferrite evident at prior austenite grain boundaries. There was slightly more grain boundary ferrite and ferrite with second phase observed in the series B welds. The presence of martensite-austenite (M-A) microphase was observed in all welds. A slight coarsening of the overall structure occurred at the highest 4 kJ/mm energy input for both the series A and B welds. These microstructural observations are consistent with the microhardness measurements listed in Table 5. In general there was a small decrease in hardness with increasing energy input.

The microstructure of the reheated regions is shown typically in Fig. 4. The structure of the series A and B welds, shown typicaly in Fig. 4(a) and (b), contained mainly acicular ferrite structure delineated by grain boundary ferrite and ferrite with second phase.

The microstructures of the CGHAZ adjacent to the fusion line are shown in Fig. 5 for the 2, 3 and 4 kJ/mm energy inputs. For the lowest 2 kJ/mm energy input, the microstructure consisted of a mixture of bainite with some regions of

low carbon martensite. At the higher energy inputs ≥3 kJ/mm a predominantly coarse upper-bainite structure was formed. The bainite consisted of packets of parallel bainitic-ferrite laths separated by islands of M-A microphases. The bainitic packets increased in size with increasing energy input. These microstructural observations are in general agreement with the recent work of Krishnadev et al. (8) who examined the microstructures of the Gleeble-simulated CGHAZ for the HSLA80 steel.

Weld Metal and CGHAZ Mechanical Properties

The tensile properties of the experimental welds are listed in Table 6. In general there was no significant difference in properties between the series A and B welds. All welds met or exceeded the minimum yield strength requirement of 565 MPa, with the exception of weld SA40. A trend to decreasing yield strength with increasing energy input was observed for both series A and B welds. Weld metal hardness also decreased slightly with increasing energy input as shown in Table 5.

The results from weld metal Charpy impact testing are presented in Fig. 6. All welds exceeded the targeted toughness requirements of 47 J at -50°C and 81 J at -18°C. For both series A and B welds, the 4 kJ/mm welds exhibited consistently higher impact energies at temperatures ≤ -40°C. This trend towards higher impact energy as energy input is increased was also observed by Jesseman and Schmid (9) who studied submerged-arc welding of A710 Grade A alloy steel.

In terms of ductile fracture all welds exhibited fully ductile behaviour at the 20°C impact testing temperature, while the 4 kJ/mm welds displayed ductility down to -20°C.

Charpy impact transition curves generated for the CGHAZ (notched 1 mm from the fusion line) of the series A weldments are shown in Fig. 7. Increasing energy input resulted in a displacement of the Charpy transition curves to higher temperatures. All welds, however, exceeded the impact requirements. The loss in toughness with increasing energy input was less dramatic than that reported by Krishnadev et al (8) who performed impact testing on Gleeble-simulated CGHAZ of HSLA80 steel samples cycled to represent 2 and 4 kJ/mm energy inputs. In general, this may be explained on the basis of the essential difference between the simulated and real weld impact tests. In the case of the real weld the Charpy notch tip resides in the CGHAZ as well as portions of the weld metal and base metal. The notch in the Gleeble specimen samples the total CGHAZ structure.

DISCUSSION

The present studies on submerged-arc welding of precipitation hardened HSLA80 have shown that both weld metal and heat-affected zone (HAZ) mechanical properties can be achieved using the currently available HY80 consumables for the energy input range of 2-4 kJ/mm. There was, however, a significant decrease in weld metal yield strength and a corresponding increase in notch toughness associated with the highest 4 kJ/mm energy input. In contrast, a decrease in HAZ notch toughness with increasing energy input was observed. However, in all cases the targeted notch toughness of 47 J at -50°C and 81 J at -18°C were met or exceeded for weld metal and HAZ. In general, these results can be explained in terms of the microstructural characteristics of the weld metal and CGHAZ regions as they are affected by increasing energy input.

The overall superior low temperature notch toughness of the weld metal was related primarily to the high proportion of acicular ferrite. The low carbon content combined with the hardenability contributions from the Mn, Ni, Cr and Mo allows the transformation of austenite to take place at sufficiently low temperatures to provide a minimum amount of grain boundary ferrite and a high percentage of fine, acicular ferrite in the range of cooling rates for energy inputs from 2 to 4 kJ/mm. The oxygen levels, listed in Table 4, are in the optimum range where, as oxide inclusions, they can act as nucleation sites for acicular ferrite formation (10).

The change in weld strength with energy input may be attributable, in part, to a precipation of copper. As indicated in Table 4 the dilution with the base metal has resulted in copper contents ranging from 0.27 to 0.65% in the weld metal. In the as-deposited region of a single pass weld copper diluted from the base metal would be primarily in solid solution. However, in multipass welds portions of the weld metal subjected to the tempering effects of subsequent weld beads could result in the formation of copper precipitates. This should be more prevalent in the 2 kJ/mm multipass welds where the number of weld beads was greater than in the 4 kJ/mm welds. Transmission electron microscopy is being carried out to confirm the precipitation of copper in the welds. Thus, it is proposed that the higher strength in the 2 kJ/mm welds compared with the 4 kJ/mm welds may be accounted for by the precipation of copper in the low energy input

welds and a slightly finer grain size. The strengthening effect of copper precipitation in the 2 kJ/mm welds is likely responsible for the lower toughness compared to the 4 kJ/mm welds.

Although the CGHAZ Charpy results exceeded the targeted values, a general trend to decreasing notch toughness was observed for increasing energy input (Fig. 7). In order to explain the change in notch toughness properties with energy input one must take into account the microstructural constituents in the region of the notch of the Charpy impact test specimen. For the CGHAZ impact test the notch is located next to the fusion line (Fig. 1b) therefore, sampling several microstructural regions including weld metal, CGHAZ and base metal. Thus the measured notch toughness will include the sum of the individual contributions of these regions. At the low energy input the CGHAZ region is small and represents only about 10-20% of the total fractured area. Thus, at 2 kJ/mm energy input the high toughness contributions of the acicular ferrite weld metal, the fine-grained polygonal ferrite base metal (5) combined with the low carbon martensite/bainite HAZ (Fig. 5(a) and ref. (8)) result in the superior low temperature toughness measured by the CGHAZ impact test. Scanning electron microscopy (SEM) confirms the presence of low carbon martensite by revealing the presence of step-like facets 5 to 10μm wide as shown in Fig. 8(a).

At higher energy inputs (4 kJ/mm) the CGHAZ region comprises 30 to 50% of the fractured area. This region was observed as a band containing large cleavage facets 40 to 80μm (Fig. 7(b)) in the SEM examination of the fractured surface of the Charpy specimens. It has been shown from Gleeble simulation studies (8) that the coarse bainitic structure of the CGHAZ region has very low cleavage fracture resistance. This low toughness component is mainly responsible for the overall reduced toughness exhibited in the CGHAZ impact test (Fig. 7) at 4 kJ/mm. This reduction in toughness contributed by the CGHAZ region was partially offset by the improved toughness of the weld metal region exhibited (Fig. 6) at 4 kJ/mm.

CONCLUSIONS

1. Submerged arc welds deposited with commercially available welding consumables in the energy input range of 2-4 kJ/mm exceeded the targeted notch toughness (81 J at -18°C and 47 J at -50°C) properties.

2. The superior weld metal notch toughness properties were attributable to the high proportion of acicular ferrite microstructure combined with the low inclusion content (O+S $\leq$ 0.0315%).
3. Although the yield strength of the welds achieved the targeted level of 565 MPa, the tendency to lower strength with increasing energy input was caused by the slight coarsening of the weld metal microstructure and a possible reduction in copper precipitation hardening at higher energy inputs.
4. The decrease in notch toughness in the CGHAZ as the energy input was increased resulted from the microstructure changing from low carbon martensite/bainite to coarse upper bainite.

ACKNOWLEDGEMENTS

The authors would like to thank Mr. D. Dolan for preparation of welds and Miss J. Ng-Yelim for the characterization of weld precipitates by electron microscopy.

REFERENCES

1. McGrath, J.T., Gianetto, J.A., Orr, R.F. and Letts, M.W., Some Factors Affecting the Notch Toughness Properties of High Strength HY80 Weldments, accepted for publication in Canadian Metallurgical Quarterly, 1987.
2. McGrath, J.T., Gianetto, J.A., Orr, R.F. and Dolan, D.E., The Development of Welding Procedures for Joining of High Strength HY100 Steel, PMRL Report 86-67(INT), 1986.
3. Kvidahl, L.D., An Improved High Yield Strength Steel for Shipbuilding, Weld. J., Vol. 64, No. 7, July 1985, pp. 42-48.
4. Jesseman, R.J. and Murphy, G.J., Mechanical Properties and Precipitation Hardening Response in ASTM A710 Grade A and A736 Alloy Steel Plates, Int. Conf. on Technology and Applications of High Strength Low Alloy (HSLA) Steels, Philadelphia, 1983, pp. 655-666.
5. Krishnadev, M.R., Development and Characterization of a New Family of HSLA Steels, HSLA Steels, Technology and Applications (Metals Park, Ohio, ASM), 1984, pp. 129-148.
6. U.S. Dept. of Defence, Military Standard MIL-E-23765/2C (SH), June 1983.
7. U.S. Dept. of Defence, Military Standard MIL-STD-1688 (SH) 1981.
8. Krishnadev, M.R., McGrath, J.T., Bowker, J.T., Dionne, S and Lassravini, A., HAZ Microstructure and Toughness of Precipitation Strengthed HSLA Steels and Conventional HY-Grade High Strength Steels, presented at AIME Int. Symposium on Welding Metallurgy of Structural Steels, Denver, Colorado, February 1987.
9. Jesseman, R.J. and Schmid, G.C., Submerged Arc Welding a Low-Carbon Copper-Strengthened Alloy Steel, Weld. J., Vol. 62, No. 11, Nov. 1983, pp. 321s-330s.
10. Cochrane, R.C. and Kirkwood, R.P., 1978, The Effect of Oxygen on Weld Metal Microstructure, Trends in Steel and Consumables for Welding, The Welding Institute, Paper 35, pp. 103-121.

Table 1. Chemical composition of HSLA80 high-strength steel

Element wt %										
C	Mn	Si	S	P	Ni	Cr	Mo	Cu	V	Nb
0.060	0.50	0.27	0.004	0.007	0.92	0.66	0.25	1.02	0.005	0.044

Table 2. Mechanical property requirements for HSLA80 submerged-arc weld metals

Ultimate Tensile Strength	For Information Only
Yield Strength	565 MPa min
Reduction in Area	50 % min
Elongation	20 % min
Charpy Impact Energy	81J at -18°C
	47J at -50°C

Table 3. Submerged arc welding consumables and parameters used for welding HSLA80

Series	Weld No.	Heat Input (kJ/mm)	Wire/Flux Combination	Current (amps)	Wire Feed Speed (mm/s)	Travel Speed (mm/s)
A	SA20	2	Linde 95/	450	55.0	7.8
	SA30	3	Oerlikon OP121TT	500	61.2	5.9
	SA40	4		570	76.2	5.1
B	SA21	2	Lincoln LA100/	450	55.0	7.8
	SA31	3	Lincoln 880 M	500	61.2	5.9
	SA41	4		570	76.2	5.1

Note: (i) voltage setting = 35 V
(ii) electrode extension = 32 mm
(iii) preheat temperature = 93°C
(iv) interpass temperature = 149°C
(v) electrode diameter = 2.4 mm

Table 4. Chemical composition of submerged arc welds and wires

Series	Weld No.	Element wt %												
		C	Mn	Si	S	P	Ni	Cr	Mo	Al	Cu	Nb	N	O
A	SA20	0.06	1.16	0.37	0.005	0.010	1.67	0.41	0.32	0.015	0.27	0.020	0.0086	0.0307
	SA30	0.05	1.14	0.37	0.005	0.010	1.43	0.32	0.29	0.015	0.45	0.020	0.0090	0.0282
	SA40	0.06	1.05	0.35	0.005	0.010	1.30	0.43	0.29	0.015	0.59	0.020	0.0109	0.0259
B	SA21	0.05	1.11	0.35	0.003	0.007	1.52	0.36	0.28	0.010	0.55	0.020	0.0094	0.0310
	SA31	0.05	1.13	0.35	0.003	0.007	1.32	0.36	0.28	0.010	0.60	0.020	0.0095	0.0274
	SA41	0.05	1.08	0.35	0.003	0.007	1.28	0.41	0.28	0.010	0.65	0.020	0.0094	0.0221
Linde 95 Wire A		0.08	1.64	0.30	0.008	0.007	1.74	0.08	0.28	0.021	0.02	<0.001	-	-
Lincoln LA100 Wire B		0.07	1.57	0.52	0.004	0.004	1.86	0.03	0.28	0.009	0.06	<0.001	-	-

Table 5. Microhardness results of HSLA80 weldments

Weld No.	Heat Input (kJ/mm)	DPH	
		Coarse Grain HAZ	Weld Metal
SA20	2	276	255
SA30	3	265	254
SA40	4	249	251
SA21	2	273	247
SA31	3	242	235
SA41	4	236	231

Table 6. Tensile properties of submerged arc weld metals

Weld No.	Yield Strength MPa	Ultimate Strength MPa	Elongation %	Reduction in Area %
SA20	658	714	27	72
SA30	604	698	25	72
SA40	564	718	24	63
SA21	669	750	27	72
SA31	603	733	25	72
SA41	565	709	29	74

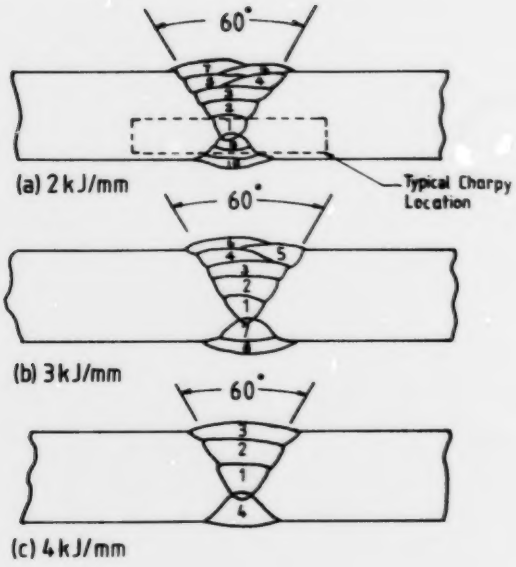

(a) Joint design preparation, pass sequence and Charpy specimen location for submerged-arc HSLA80 weldments. (neg 15466)

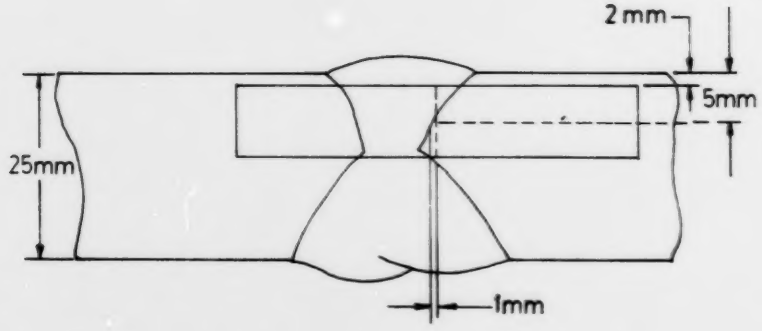

(b) Schematic diagram showing position of HAZ Charpy test specimen, notched through thickness 1 mm from fusion line. (neg 14093)

Fig. 1.

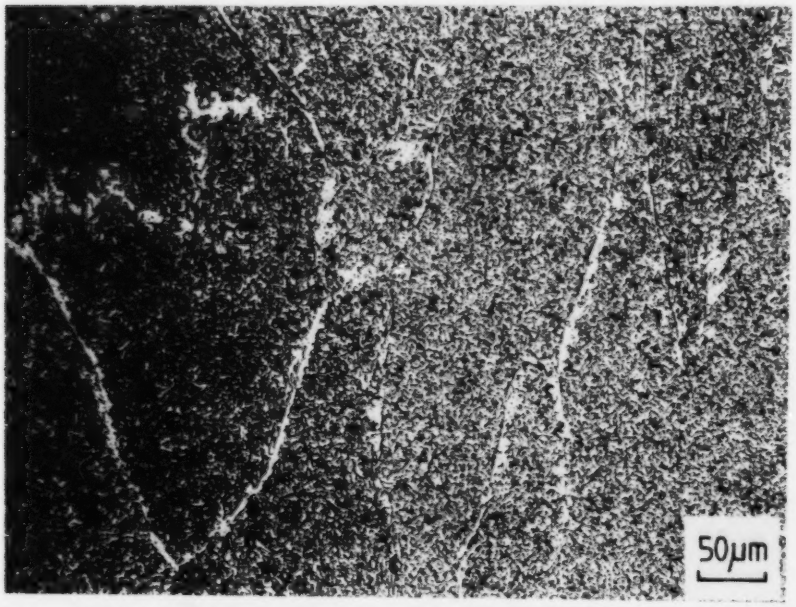

(a) SA20, columnar structure (neg 15596)

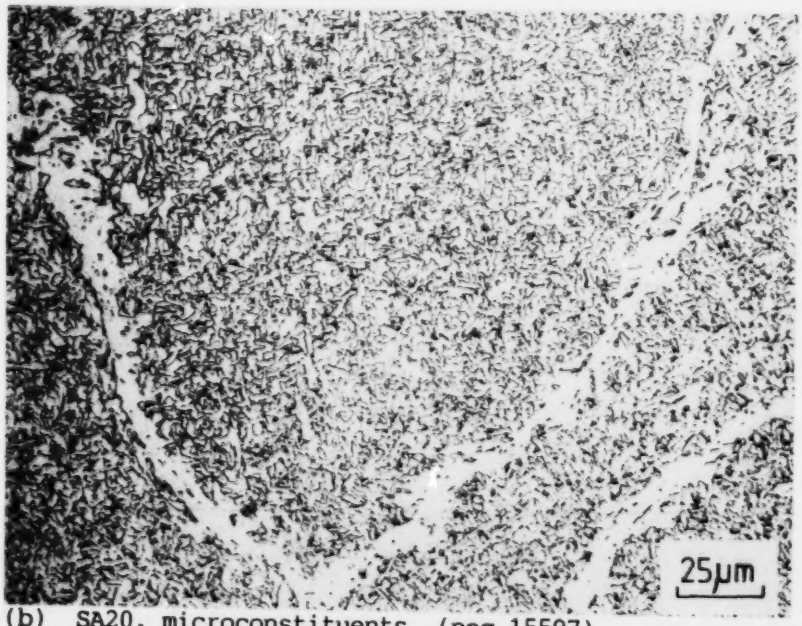

(b) SA20, microconstituents (neg 15597)

Fig. 2. cont'd

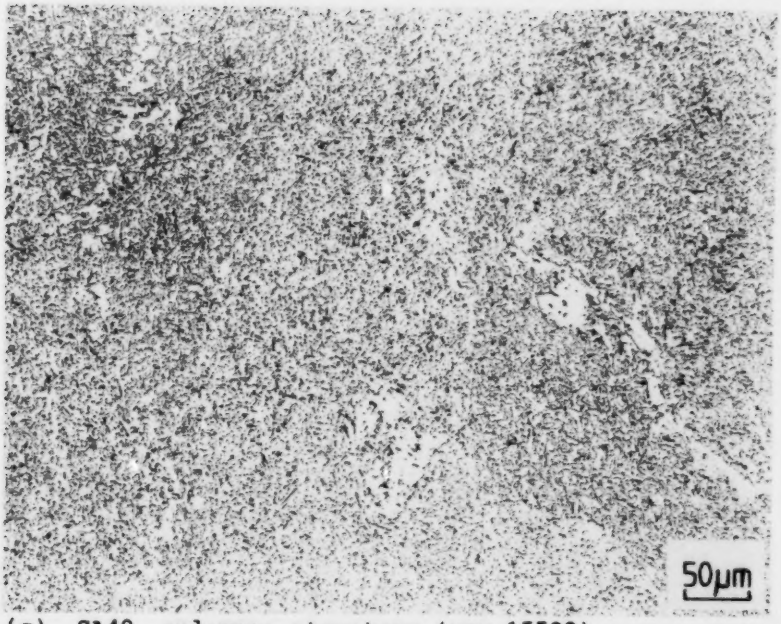

(c) SA40, columnar structure (neg 15598)

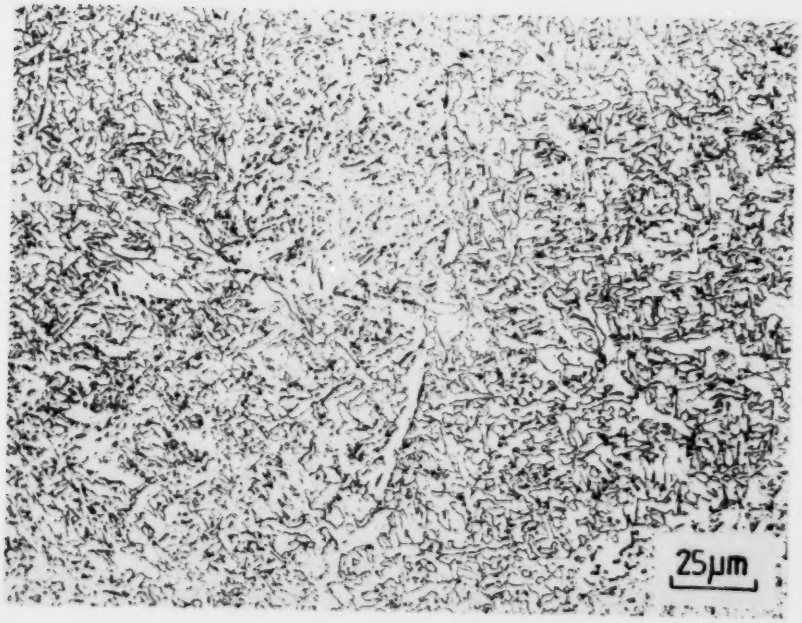

(d) SA40, microconstituents (neg 15599)

Fig. 2. Weld metal microstructures of submerged-arc welds deposited with Series A Linde 95/Oerlikon OP121TT consumables.

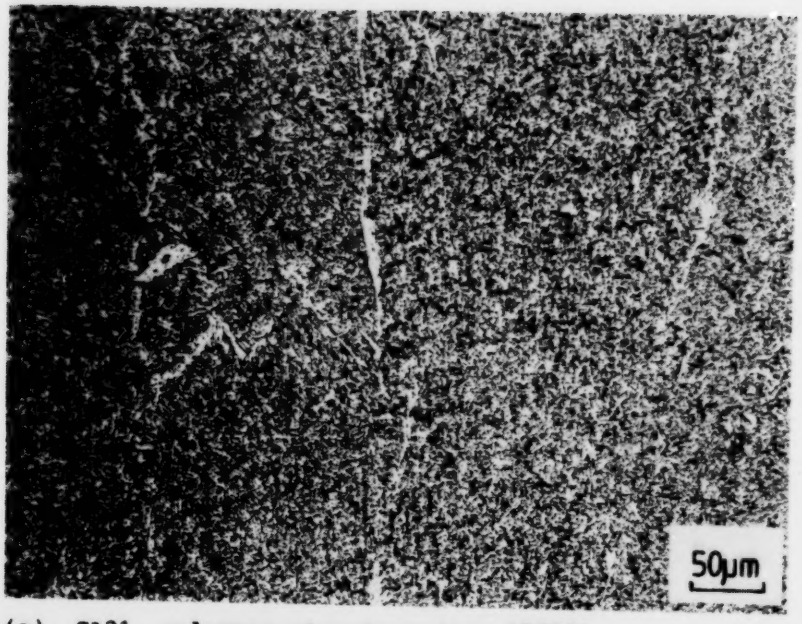

(a) SA21, columnar structure (neg 15600)

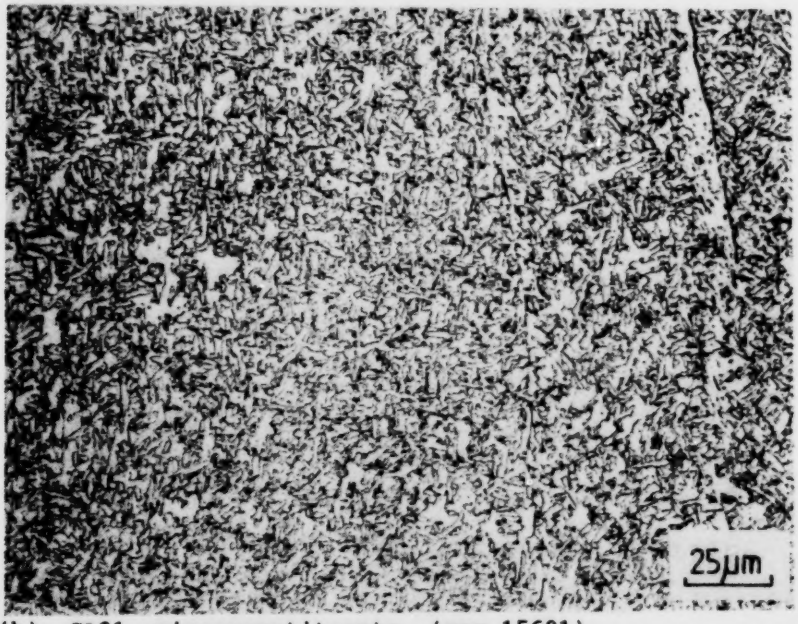

(b) SA21, microconstituents (neg 15601)

Fig. 3. cont'd.

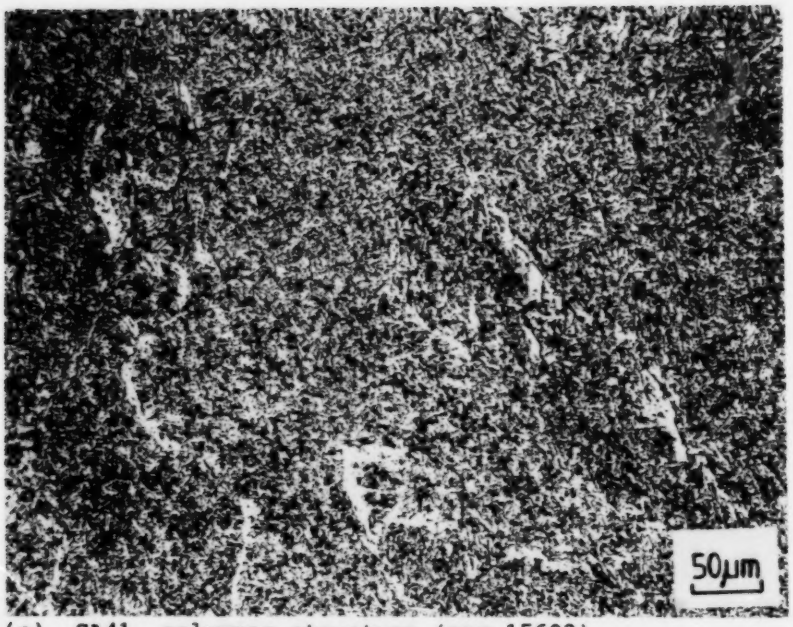

(c) SA41, columnar structure (neg 15602)

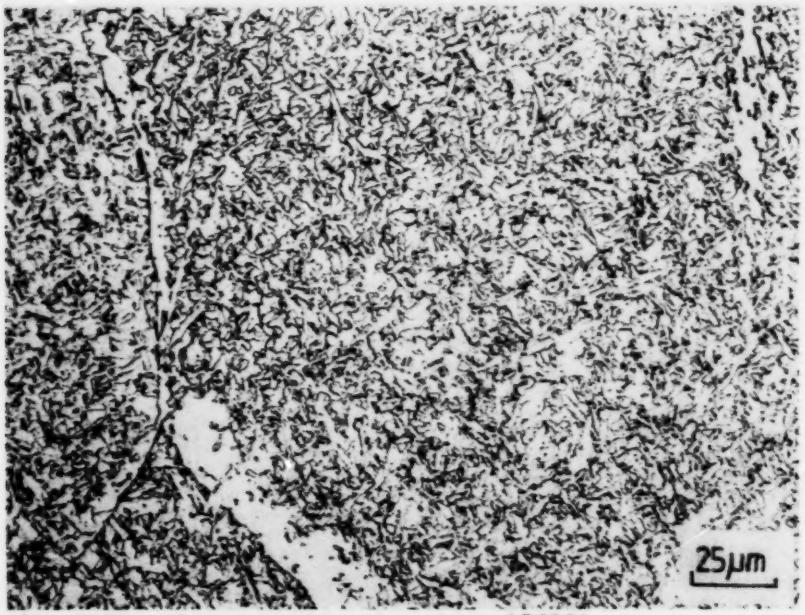

(d) SA41, microconstituents (neg 15603)

Fig. 3. Weld metal microstructures of submerged-arc welds deposited with Series B Lincoln LA100/880M consumables.

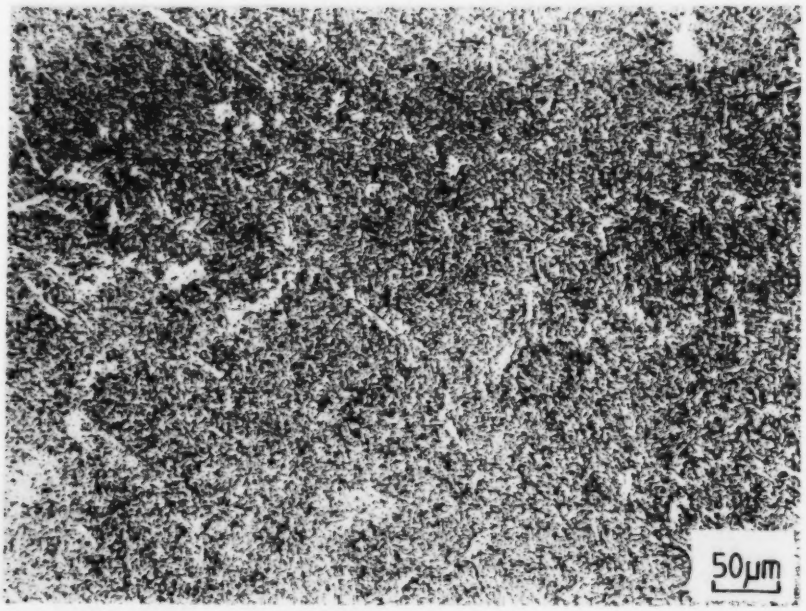

(a) Weld SA20 (neg 15604)

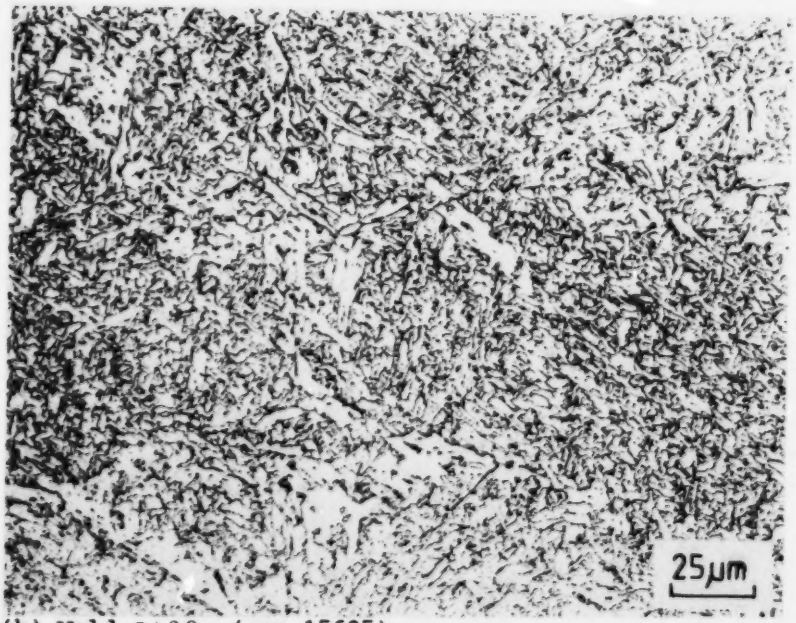

(b) Weld SA2C (neg 15605)

Fig. 4. Microstructures of reheated weld metal regions in submerged-arc welds deposited at 2 kJ/mm

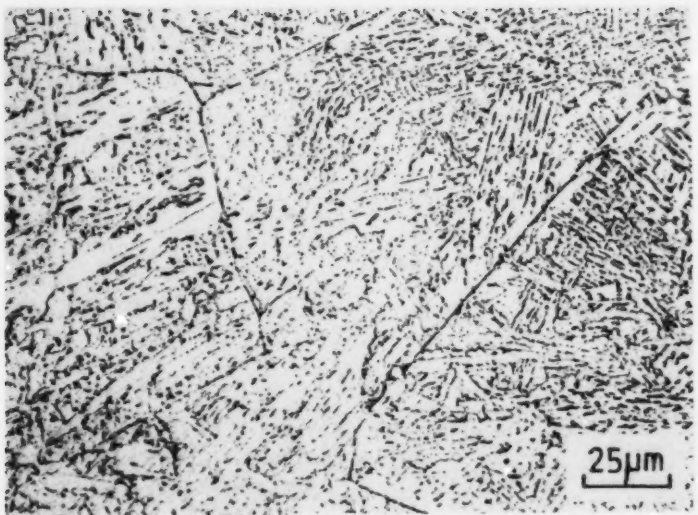

(a) 2 kJ/mm (15606)

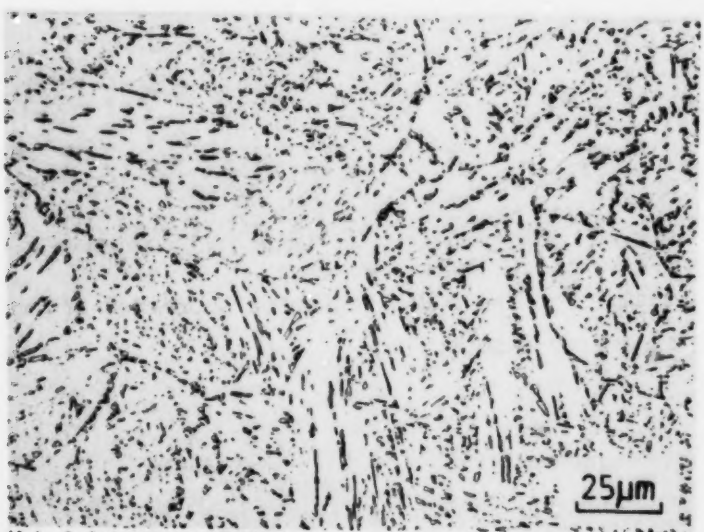

(b) 3 kJ/mm (15607)

Fig. 5. cont'd.

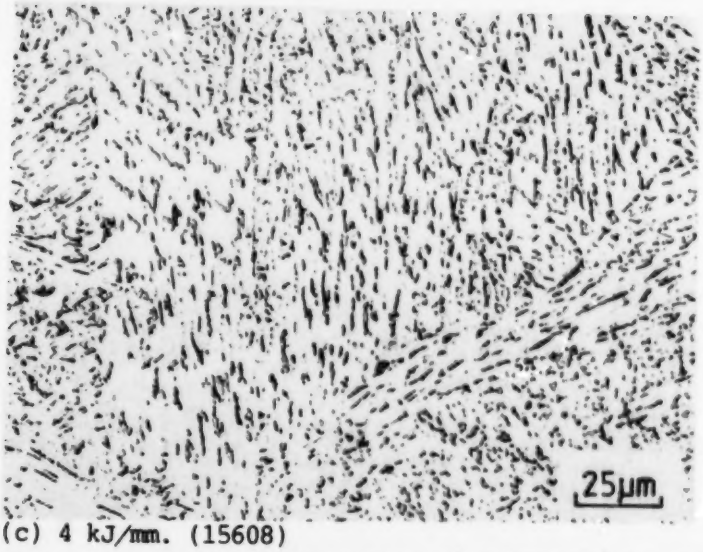

(c) 4 kJ/mm. (15608)

Fig. 5. Microstructures of the CGHAZ region of submerged-arc welds deposited at a range of energy inputs.

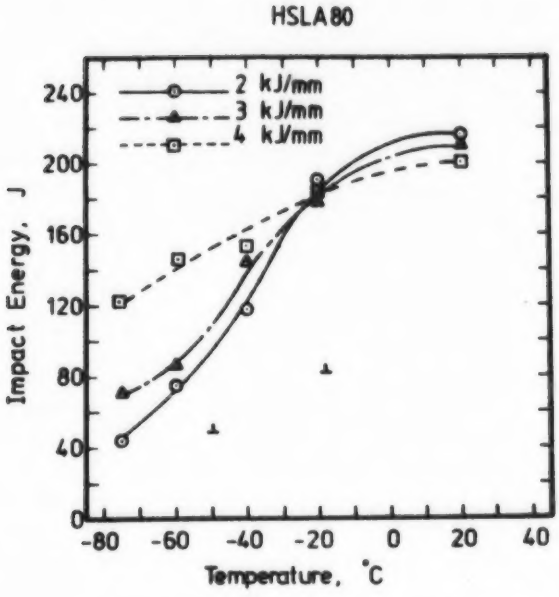

(a) Series A - Linde 95 / Oerlikon OP121 TT

(a) (neg 15467)

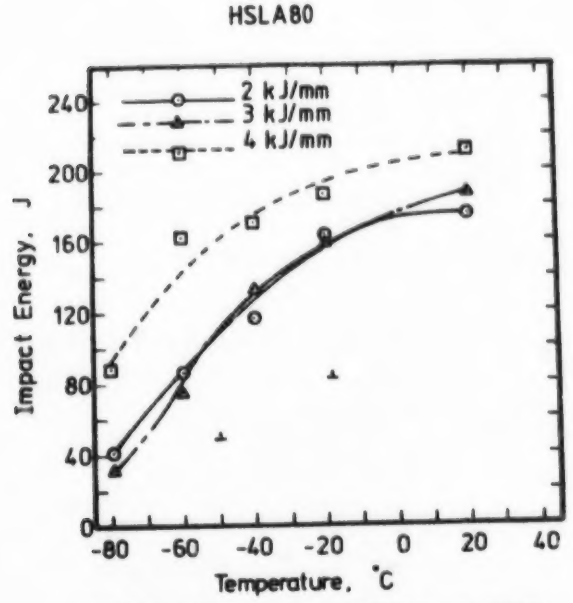

(b) Series B - Lincoln LA100/ Lincoln 880M

(b) (neg 15464)

Fig. 6. Charpy transition curves of submerged-arc weld metals deposited at a range of energy inputs. The targeted notch toughnesses are indicated by the ⊥ symbol.

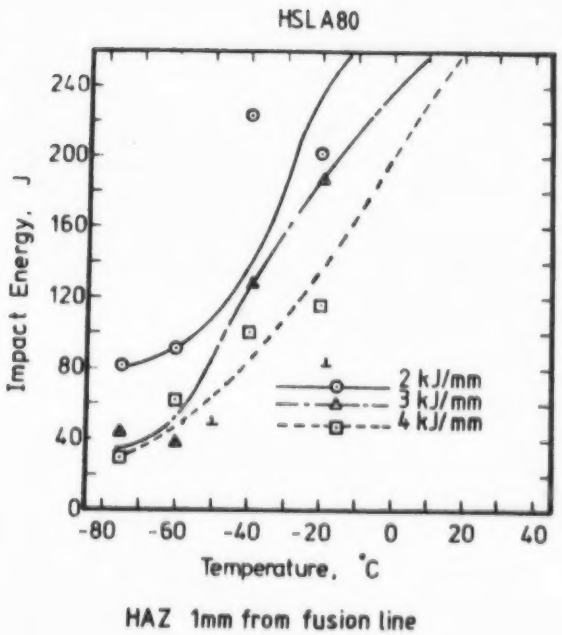

Fig. 7. Charpy transition curves for CGHAZ specimens notched 1 mm from the fusion line in HSLA80 steel. The targeted notch toughnesses are indicated by the ⊥ symbol. (neg 15465)

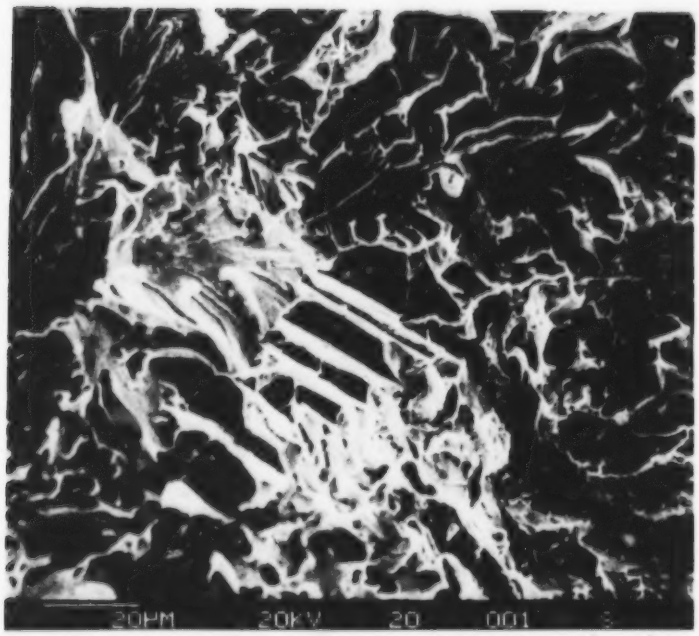

(a) Fractograph of 2 kJ/mm Charpy specimen showing cleavage facets corresponding to the mixed bainite and low carbon martensite microstructure.

(b) Cleavage facets of the 4 kJ/mm Charpy specimen corresponding to the coarse upper bainite microstructure.

Fig. 8. SEM fractographs of fractured surfaces of Charpy specimens takes 1 mm from the fusion line in HSLA80 welds.